Propulsion and Power Research 2015;4(4):190–201

HOSTED BY

ELSEVIER

http://ppr.buaa.edu.cn/

Propulsion and Power Research

www.sciencedirect.com

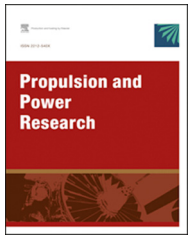

ORIGINAL ARTICLE

Film cooling adiabatic effectiveness measurements of pressure side trailing edge cooling configurations

R. Becchi[a], B. Facchini[a], A. Picchi[a,*], L. Tarchi[a], D. Coutandin[b], S. Zecchi[b]

[a]*Department of Industrial Engineering, University of Florence, Via S. Marta 3, 50139, Firenze, Italy*
[b]*GE Avio S.r.l., Via I Maggio 99, 10040, Rivalta di Torino, Torino, Italy*

Received 12 September 2014; accepted 5 May 2015
Available online 28 November 2015

KEYWORDS

Turbine blades;
Trailing edge;
Film cooling;
Pressure sensitive paint (PSP)

Abstract Nowadays total inlet temperature of gas turbine is far above the permissible metal temperature; as a consequence, advanced cooling techniques must be applied to protect from thermal stresses, oxidation and corrosion the components located in the high pressure stages, such as the blade trailing edge. A suitable design of the cooling system for the trailing edge has to cope with geometric constraints and aerodynamic demands; state-of-the-art of cooling concepts often use film cooling on blade pressure side: the air taken from last compressor stages is ejected through discrete holes or slots to provide a cold layer between hot mainstream and the blade surface. With the goal of ensuring a satisfactory lifetime of blades, the design of efficient trailing edge film cooling schemes and, moreover, the possibility to check carefully their behavior, are hence necessary to guarantee an appropriate metal temperature distribution. For this purpose an experimental survey was carried out to investigate the film covering performance of different pressure side trailing edge cooling systems for turbine blades. The experimental test section consists of a scaled-up trailing edge model installed in an open loop suction type test rig. Measurements of adiabatic effectiveness distributions were carried out on three trailing edge cooling system configurations. The baseline geometry is composed by inclined slots separated by elongated pedestals; the second geometry shares the same cutback configuration, with an additional row of circular film cooling holes located upstream; the third model is equipped with three rows of in-line film cooling holes. Experiments have been performed at nearly ambient conditions imposing several blowing ratio values and using carbon dioxide as coolant in order to reproduce a density ratio close to the engine conditions ($DR = 1.52$). To extend the validity of the survey a comparison between adiabatic effectiveness

*Corresponding author. Tel.: +39 055 8827649.
E-mail address: alessio.picchi@htc.de.unifi.it (A. Picchi).

Peer review under responsibility of National Laboratory for Aeronautics and Astronautics, China.

http://dx.doi.org/10.1016/j.jppr.2015.10.001

measurements and a prediction by correlative approach was performed to compare the experimental results with 1D methodologies.

1. Introduction

The engine cycle efficiency is directly linked to the peak temperature of the working fluid, that affect the gas path, currently above the maximum allowable metal temperature. Design of the trailing edge (TE) blade cooling system is nowadays challenging due to the geometric constraints in combination with aerodynamic demands and structural integrity.

For high thermally loaded blades, a combination of internal and external cooling systems are employed at blade trailing edge to guarantee wall temperatures within the limits prescribed by structural integrity. The current state of the art of trailing edge cooling systems often use schemes where cooling air, used to provide an internal convective cooling, is ejected onto the pressure side trough spanwise slots, also called cutback, or film holes. The unsteady interaction between coolant and main flow and its effect on cooling performance are difficult to be predicted; as a consequence, the adiabatic effectiveness distributions on the trailing edge pressure side are generally hard to estimate with sufficient accuracy using classical simplified correlations, which may lead to high overestimation of the cooling rates and, above all, makes difficult the optimization of the cooling system.

In the technical literature several works were presented regarding the characterization of trailing edge cooling devices at blade pressure side. An extensive survey was presented by Holloway et al. [1,2]: they combined both numerical computations and experiments to investigate pressure side bleed on the trailing edge of a turbine blade. The vortex shedding at the slots lip was identified as the key mechanism for the mixing of coolant and hot gas and the major responsible of effectiveness decay for cutback with high lip thickness. A follow-on to their study was conducted by Medic and Durbin [3] who analysed the primary role of natural and forced unsteadiness in trailing edge cooling flows by means of unsteady Reynolds averaged Navier-Stokes (RANS) computations. More recently, further numerical studies on trailing edge cooling performance were carried out by Schneider et al. [4] and Joo and Durbin [5] by employing respectively a large eddy simulation (LES) matched with an existing experimental set-up and an hybrid RANS/LES approach.

Concerning experimental works on film effectiveness at blade trailing edge, a pioneering study was conducted by Taslim et al. [6] testing different slot models varying the exit configuration. The results showed that film effectiveness is mainly affected by slot lip thickness to height ratio, while slot width to height ratio and density ratio represent less sensitive parameters. More recently, Martini et al. [7] evaluated, by means of an infra-red technique, heat transfer coefficients and the film effectiveness of a cutback trailing edge model for different internal cooling arrangements. Results suggested a dominant role of the mixing process generated at the ejection lip on film covering. In continuation of this work the same research group performed deepened investigations [8,9] on the effects of different slot lip geometries. In terms of adiabatic effectiveness, results highlighted a strong dependency on ejection lip thickness, while minor improvements are obtained with a rounded ejection lip profile. Film cooling efficiency on the surface of the pressure side trailing edge area for two TE configurations was determined by Dannhauer [10] using an infra-red thermography technique. Yang and Hu [11] carried out an experimental campaign to measure the adiabatic cooling effectiveness distribution over the protected surface in the breakout region of a turbine blade trailing edge model. Tests were performed by means of the pressure sensitive paint (PSP) technique, and were coupled with detailed flow field measurements in order to optimize design parameters for improved cooling performances.

Several works focused on both the aerodynamic and thermal issues associated with trailing edge cooling. An extensive analysis on two typical TE geometries was conducted by the University of North Dakota [12–15] in a large scale cascade composed by a four vane three full passage arrangement. For a gill slot configuration equipped with a pin fin array, authors found high adiabatic effectiveness levels at the slot exit, however up to 4 cm downstream the injection protection tends to dissipate toward the trailing edge, suggesting an interaction with the shedding. From an aerodynamic perspective, the gill slot produces a total pressure loss, at design and near design flow conditions, rather higher than a solid base reference vane. At design flow, this loss decreases with increasing Reynolds number. In the case of a letterbox trailing edge, obtained adding flow partitions to the previous geometry, film cooling protection is reduced with respect to gill slot. The letterbox configuration has achieved smaller total pressure losses compared with the gill slot. However, the letterbox needs an increased pressure drop for equal ejection flow. Barigozzi et al. [16] investigated a trailing edge cooling configuration featuring a pressure side cutback with film cooling slots and two rows of holes placed upstream of the cutback. Downstream of the cooling holes, the highest adiabatic effectiveness level can be reached for a mass flow ratio equal to 1.2%. Downstream

Nomenclature

A	surface (unit: m^2)
BR	blowing ratio
C	oxygen concentration
d	holes diameter (unit: mm)
D	pin fins diameter (unit: mm)
DR	density ratio
h	slot height (unit: mm)
I	intensity (unit: counts)
$L_{\eta_{ad}>0.9}$	core region length (unit: mm)
M	molecular weight (unit: kg/kmol)
$\dot{m}$	mass flow (unit: kg/s)
P	pressure (unit: Pa)
Re	Reynolds number
S_x	streamwise pitch (unit: mm)
S_y	spanwise pitch (unit: mm)
t	lip thickness (unit: mm)
w	slot width (unit: mm)
T	temperature (unit: K)
U	velocity (unit: m/s)
x	streamwise direction (unit: mm)
y	spanwise direction (unit: mm)

Greek letters

η	effectiveness
μ	dynamic viscosity (unit: kg/(m · s))
ρ	density (unit: kg/m^3)

Subscripts

ad	adiabatic
air	air injection
cool	cooling flow
dark	led switched off
fg	foreign gas
holes	coolant through holes
main	mainstream
max	maximum
O_2	oxygen
ref	reference
slot	slot flow
w	wall

Acronyms

CCD	charge coupled device
FIB	fluoro isopropyl butyl
LES	large eddy simulation
PMMA	poly-methyl methacrylate
PSP	pressure sensitive paint
RANS	Reynolds averaged Navier-Stokes
TE	trailing edge
UV	ultra-violet

of the slot exit up to the trailing edge, an increase in the mass flow rate improves the film protection. Not significant variations in boundary layer behavior were highlighted in the range of tested isentropic exit Mach numbers.

Despite the interest in that topic, to the authors' knowledge there are only a very few works, in open literature, aimed at comparing different trailing edge cooling arrangement with detailed 2D maps on the whole pressure side model surface. Moreover, a comparative study of different trailing edge models is considered of outstanding importance to support the design and to help the selection of the proper cooling configuration. For these reasons, the aim of the present paper is the evaluation of adiabatic effectiveness distributions on three different trailing edge film cooling models. The first model represents the pressure side cutback equipped with elongated pedestals; the second model shares the same features of the previous design including also a row of tilted holes; finally the last model is equipped with three rows of tilted in-line holes. Tests were carried out by means of PSP technique using CO_2 as cooling flow, in order to reproduce a density ratio (DR) close to engine; the PSP technique, based on the heat and mass transfer analogy, has allowed to catch detailed 2D effectiveness distributions on the whole trailing edge surface including the pedestals external surfaces. Tests have been performed imposing several values of cooling system blowing ratio and replicating the Reynolds numbers of mainstream and cooling flows.

Results were discussed by cross-comparing the film covering performance of the three geometries, in order to highlight pros and cons of each cooling system. To extend the survey, a correlative analysis was performed to stress the applicability of Sellers' superposition approach [17] to predict the film distribution in case of multiple injection of coolant through holes and slots.

2. Experimental setup

2.1. Test facility

The experimental apparatus, depicted in Figure 1 is an open loop suction type test rig with a constant test section area (40 mm × 120 mm) which allows the complete control of three separate flows: the mainstream, the cooling flow and the flow used for the aspiration of the boundary layer at the inlet of the rig.

The mainstream is drawn by means of two vacuum pumps from the ambient; before entering into the test section, it flows through honeycombs and several screens which allow to set an uniform velocity profile at the inlet. A passive turbulence generator (parallel square bars; 4.5 mm bar thickness; 12 mm pitch), located about 400 mm upstream the test geometry, is used to achieve a turbulence level of 4.5%, at the beginning of the test model.

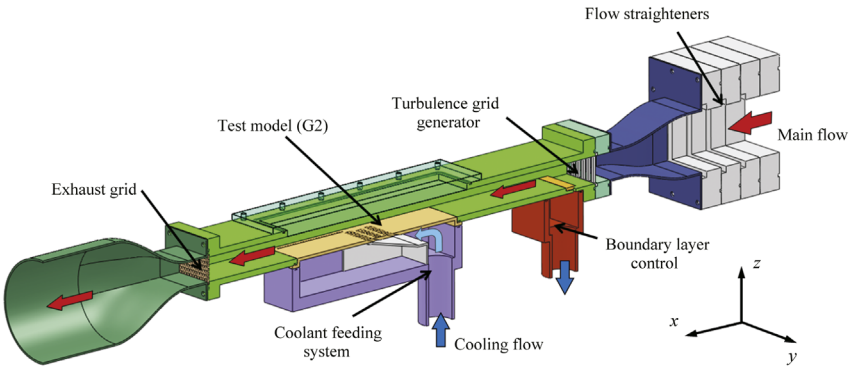

Figure 1 Cross-sectional view of the test rig.

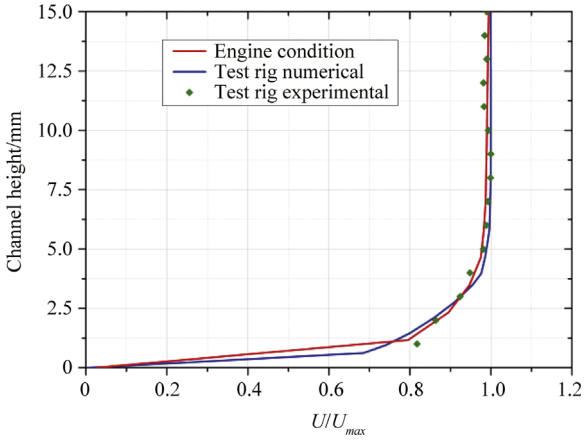

Figure 2 Boundary layer thickness.

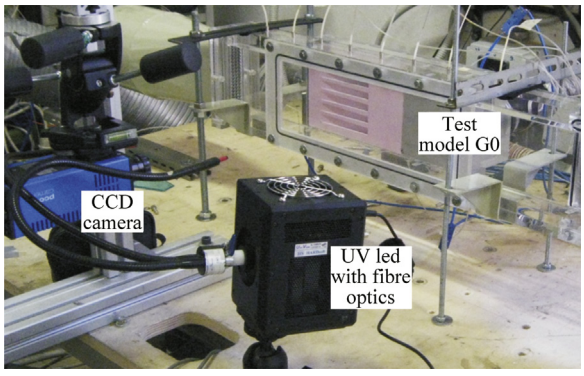

Figure 3 Experimental apparatus.

A slot with a thickness of 5 mm connected to a small plenum chamber is used to draw and to control the development of the boundary layer in the test rig. In particular, this feature guarantees the similitude with an engine boundary layer thickness. Numerical simulations performed to support the design of the test rig and following experimental measurements confirm a good agreement between the velocity profile both in the rig and at engine condition at the beginning of test section (Figure 2). During the tests, the ratio between the extracted mass flow and the total inlet mass flow has been imposed equal to about 11% according to the geometrical dimensions of the test rig (i.e. $5/45 \approx 0.11$), where 5 mm is the thickness of the slot for the boundary layer control and 45 mm is the channel height at the inlet).

Turbulence level and velocity profiles were measured using a Dantec® CTA system with a single sensor probe Dantec® 55p04 traversed along the direction normal to the trailing edge model surface. The data were sampled at 100 kHz and the sampling period was set at 1 seconds. The turbulence length scale was evaluated using the frozen turbulence approximation [18] and results show good agreement with the level predicted by the correlation proposed by Roach [19].

The central part of the test section allows to install the three different trailing edge models and the respective coolant feeding systems. The coolant is supplied by a separate line with air or carbon dioxide stored in a pressure tank ($T \approx 290$ K). The CO_2 used to feed the cooling scheme allows to reproduce a density ratio between the cooling flow and the mainstream equal to 1.52.

The mass flow rate is measured in three different locations of the rig: according to the standard EN ISO 5167-1, one orifice measures the flow rate blown by the pumps, while other two orifices measure the cooling flow and the mass flow extracted to control the development of the boundary layer. A pressure scanner Scanivalve 9116R with temperature compensated piezoresistive relative pressure sensors measures the static pressure in 16 different locations. Several T type thermocouples (uncertainty ± 0.5 K with level of confidence of 95%) connected to a data acquisition/switch unit (HP Agilent 34970A) measure the mainstream and the coolant static temperatures.

Adiabatic effectiveness measurements were performed by means of pressure sensitive paint technique, PSP used in the present work was supplied by Innovative Scientific Solutions Inc. and was composed by a blend of fluoro isopropyl butyl polymer (FIB) and platinum tetra (pentafluorophenyl) porphine. PSP was directly sprayed on the test surface with 9 very light cross coat using an air brush. The correct light source for painted surface excitation is provided by an high power ultra-violet (UV) led illuminator IL-104x, equipped with goose-neck fibre optics,

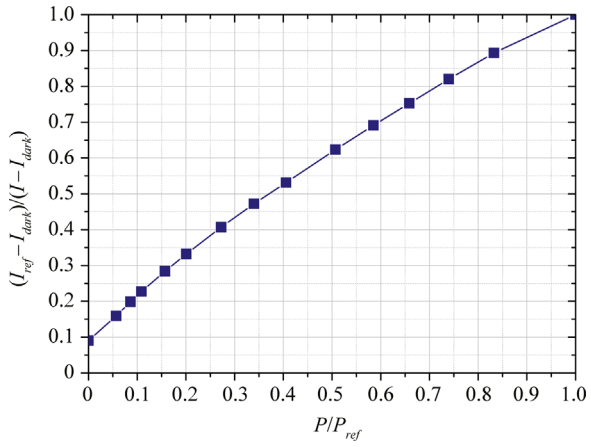

Figure 4 PSP calibration curve.

filtered with a blue band pass filter. Meanwhile, a 1600×1200 resolution 14-bit charge coupled device (CCD) camera (PCO.1600) with a 610 nm red filter records the intensity emitted by pressure sensitive paint. The test rig is completely made of transparent poly-methyl methacrylate (PMMA), thus allowing the required optical access for PSP measurements without influence the UV excitation and the emission of the paint; while the scaled up trailing edge geometries are made of aluminium. A picture of the experimental apparatus is reported in Figure 3.

2.2. Pressure sensitive paint

The PSP is an organic substance composed by oxygen sensitive molecules embedded in the paint solution using a polymer binder permeable to oxygen. Electrons in the oxygen sensitive molecules are excited to higher energy levels by an incidence UV light. On returning back to their original state, light at a lower frequency is emitted; the intensity of the light increases as the oxygen concentration in the binder around the sensitive molecules is decreased. This phenomenon takes name of oxygen quenching [20].

Assuming the analogy between heat and mass transfer, if a tracer gas without free oxygen is used as coolant in a film cooling system it is straightforward to replace the temperature definition of film cooling effectiveness by mass fractions of oxygen [21]:

$$\eta_{ad} = \frac{T_{main} - T_{ad}}{T_{main} - T_{cool}} \Rightarrow \frac{C_{main} - C_w}{C_{main}} \tag{1}$$

here C_{main} is oxygen concentration of main free stream and C_w is the oxygen concentration in proximity of the wall. The concentrations listed in the definition of adiabatic effectiveness can be estimated point by point on each test model exploiting the oxygen quenching phenomenon thanks to the PSP molecules.

Before their use in the test rig, PSP must be calibrated in order to evaluate the relation between intensity and pressure. The relation between the light emitted by the paint and the pressure for a constant temperature of about 298 K is plotted in Figure 4. The intensity field, I, corrected with the background noise (dark), and the static pressure P, are both normalized with the reference condition acquired at room conditions (I_{ref}; P_{ref}). Once the calibration is accomplished, the adiabatic effectiveness distribution using PSP steady-state technique is obtained acquiring 4 different images for each tested flow condition:

1. Image acquired with the UV illumination system switched off in order to correct the background noise.
2. Image recorded using CO_2 as tracer gas for the cooling line and air for the mainstream line at the desired flow conditions.
3. Image obtained at the same flow conditions of the previous acquisition; in this case air is employed both for mainstream and cooling lines.
4. Image captured with no flow condition, it represents the reference intensity field of the previous acquisitions.

Each image was evaluated as an average of at least 100 acquisitions captured in the same condition to reduce measurement noise; during the experiments coolant and mainstream were set at the same room temperature. In order to express Eq. (1) in terms of partial pressure of oxygen as measured with PSP, the adiabatic effectiveness formulation is elaborated using the molecular weight:

$$\eta_{ad} = 1 - \frac{1}{1 + \left(\frac{P_{O_2;air}/P_{O_2;ref}}{P_{O_2;fg}/P_{O_2;ref}} - 1\right) \cdot \frac{M_{fg}}{M_{air}}} \tag{2}$$

Exploiting the PSP calibration curve, the image acquired for each test point can be used to estimate the normalized partial pressure of oxygen in case of tracer gas and air injection through the cooling system (respectively $P_{O_2;fg}/P_{O_2;ref}$ and $P_{O_2;air}/P_{O_2;ref}$). Therefore the partial pressures of oxygen were used to estimate adiabatic effectiveness distribution pixel-by-pixel using the Eq. (2). A detailed description of the PSP technique for adiabatic effectiveness measurements has been recently reported by Caciolli et al. [22].

The uncertainty of adiabatic effectiveness measurements was evaluated based on the method proposed by Kline and McClintock [23] and on a confidence level of 95%. It is estimated to be 10% for $\eta_{ad}=0.2$ and 2% for $\eta_{ad}>0.8$, taking into account the uncertainties in calibration and image capture.

2.3. Test models and test conditions

The test matrix is composed by the three different geometries depicted in Figure 5, which represent realistic pressure side cooling schemes for airfoils trailing edge:

- **G0**: the model is characterized by 5 slots with elongated pedestals. The slots have a width to height ratio of $w/h=2.3$ and are spaced at a spanwise pitch to height ratio $S_{slot}/h=3.9$; the slot inclination angle is 5 deg. The

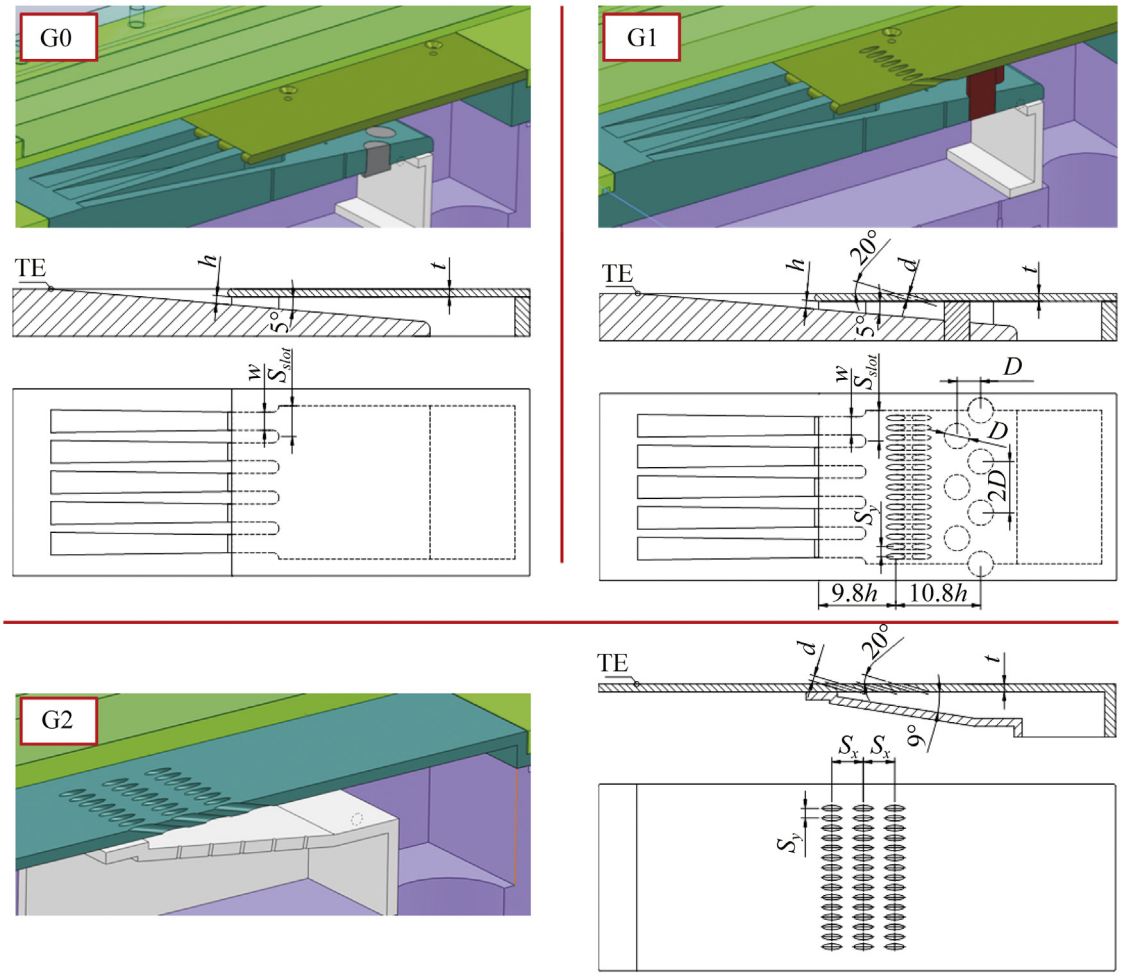

Figure 5 Trailing edge models.

Table 1 Test matrix.

Model		*BR*	*Re*
G0		0.3-1.4	7000-32000
G1	slot	0.2-1.0	5000-23000
	holes	0.15-0.75	3000-12000
G2		0.4-1.2	6000-18000

cutback has a rounded ejection lip profile and a thickness (t) to slot height ratio equal to 1.

- **G1**: in addition to the features described for geometry G0, this model presents a row of holes with a pitch to diameter ratio $S_y/d = 1.8$ and a 20 deg inclination, without compound angle. Two rows of staggered pin fins, characterized by a diameter to slot height ratio $D/h = 3.2$, are located in the internal feeding channel with a pitch in streamwise direction equal to D and in the spanwise direction equal to $2D$.
- **G2**: it is equipped with three rows of in-line circular holes with an inclination angle of 20 deg and a hole length to diameter ratio $L/d \approx 4$. The streamwise pitch to diameter ratio is $S_x/d = 5.7$ and the spanwise pitch to diameter ratio is $S_y/d = 1.8$. Feeding system is realized using a 9 deg inclined ramp inserted below the perforated plate.

The experimental campaign was performed imposing several fluid dynamics conditions ranging among typical engine values. The main investigation parameter of the test rig is the blowing ratio of slot and cooling holes:

$$BR_{slot} = \frac{(\rho \cdot U)_{slot}}{(\rho \cdot U)_{main}} \tag{3}$$

$$BR_{holes} = \frac{(\rho \cdot U)_{holes}}{(\rho \cdot U)_{main}} \tag{4}$$

For G1 geometry, *BR* and *Re* computation was executed evaluating the cooling mass flow rate split by means of a flow network solver described in the works by Bonini et al. [24] and Andrei et al. [25]. For G2 geometry a global blowing ratio for the three rows of film cooling holes was employed. No acceleration parameter has been considered in the analysis, neglecting the simulation of the pressure gradient along the rows of holes. Using the distance between the slot for boundary layer control and the beginning of the test section (about 380 mm) as the

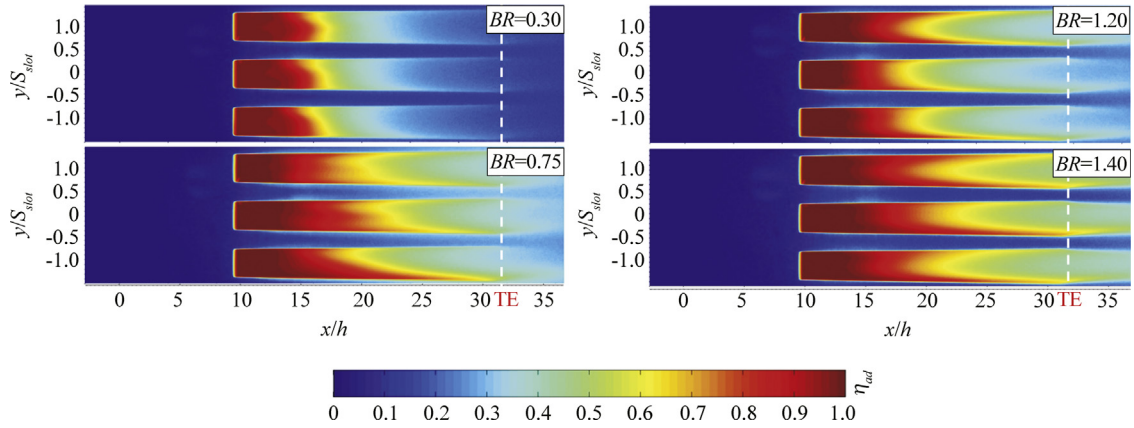

Figure 6 Adiabatic effectiveness 2D distributions (G0).

reference length, the Reynolds number of the mainstream was fixed, acting on pumps speed, at 1.5×10^6. This value is comparable with the expected Reynolds number at engine conditions, considering the distance between the leading and the trailing edge on pressure side in blade coordinate as the reference length. At the imposed condition, mainstream Mach number takes the value of 0.17. For both parameters a good stability was achieved during the entire experimental campaign, addressing a maximum variability of the order of 1.5%. In the range of the imposed blowing ratios, the Reynolds numbers of the cooling flows vary within typical engine values and are evaluated, respectively, as:

$$Re_{slot} = \frac{\dot{m}_{slot} \cdot h}{A_{slot} \cdot \mu_{cool}} \tag{5}$$

$$Re_{holes} = \frac{\dot{m}_{holes} \cdot d}{A_{holes} \cdot \mu_{cool}} \tag{6}$$

where h is the slot height and d is the holes diameter. Summarizing, in Table 1 are reported the test conditions investigated in the present works.

3. Results

Results will be reported in terms of bi-dimensional, lateral averaged and spanwise averaged distributions on the whole test surface. In the first part of the present section, a detailed analysis of the results obtained on all the trailing edge models will be presented, afterwards the work will deal with a comparison between experimental data and the results predicted by a correlative approach on geometry G1. Finally a comparison between the film performance obtained on the three geometries will be reported, normalizing the weight of the coolant consumption.

3.1. Geometry G0

The adiabatic effectiveness maps for geometry G0 for several tested conditions are reported in Figure 6, focusing on the three central slots. As a general result, all flow conditions show the presence of a core region with high effectiveness located at the slot exit ($x/h \approx 10$) and a deterioration of the film covering moving towards the outlet of the rig due to the intense mixing with the mainstream. In

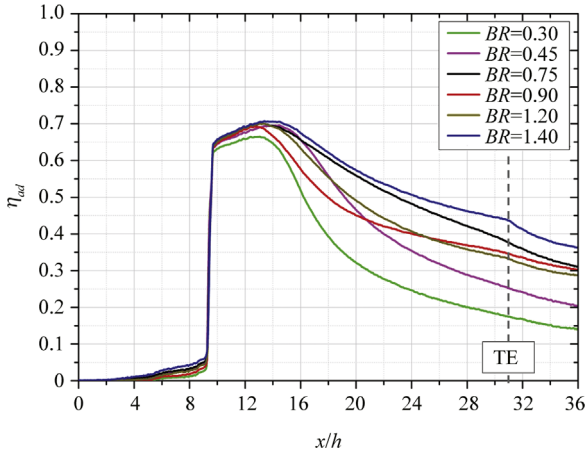

Figure 7 Geometry G0 spanwise averaged adiabatic effectiveness, including slots and pedestals, for different *BR* conditions.

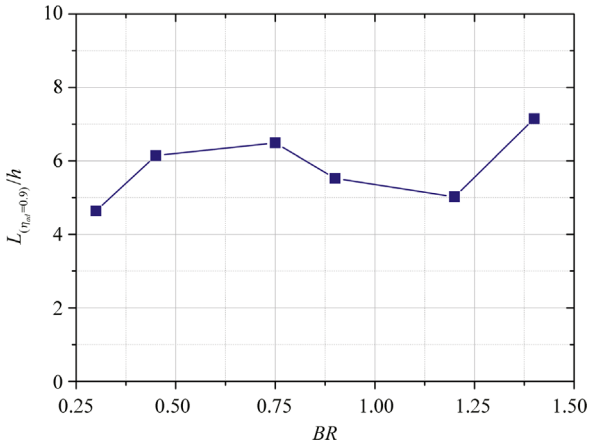

Figure 8 Streamwise length of high effectiveness region ($\eta_{ad} > 0.9$) for geometry G0, including only slots.

addition, a slight protection of the pedestal outer surface is visible for all the flow conditions.

For each condition tested a spanwise averaged effectiveness curve is computed and reported in Figure 7 including both the pedestals and the slots surface. Increasing *BR* a non-monotonic protection trend can be observed in the region immediately downstream the high effectiveness core region ($x/h \approx 20$). This behavior can be explained with the effect of vortex shedding near the slot lip that becomes more intense approaching *BR* around unity. In this condition, as confirmed by the results of Holloway et al. [2], the vortices generated at the slot lip shed off in alternating pattern, since the momentum of coolant and main flows have similar magnitude and neither vortex is dominant. This behavior leads to a drastic change in the coolant field and consequently to an appreciable reduction of film protection increasing the blowing ratio and hence the coolant consumption from $BR=0.75$ to $BR=0.9$.

This behavior is clearly evident analyzing also the length of the high effectiveness core region reported in Figure 8. The length of the core region, $L_{\eta_{ad}>0.9}$, is defined as the distance from the slot exit in the streamwise direction where the laterally averaged film cooling effectiveness, calculated on the central slot excluding the pedestal surface, decays below a level of $\eta_{ad}=0.9$. As highlighted by the 2D distributions, the length of the effective core region is generally sustained by an increase of the blowing ratio, except for the range $0.75<BR<1.25$ where the trend exhibits a local minimum.

To better understand the film behavior, the spanwise averaged film effectiveness curves are also computed focusing on the two central pedestals surface varying the blowing ratio (Figure 9). Despite the best film protection on the slot area, as reported in the 2D maps, is achieved at $BR=1.4$, the pedestal region reaches the best protection between $BR=0.75$-0.9, after which the film covering decays increasing the cooling flow. This behavior suggests that the spreading of the cooling flow, responsible of the pedestal protection, is less intense at high *BR* where the coolant is characterized by an extended potential core region. Moreover, in the investigated range of cooling parameter, the optimum of the pedestal protection is obtained for the range of blowing ratio where, as discussed above, the coolant-mainstream interaction is more severe causing a rapid decay of film effectiveness downstream the slot exits. Likely, this interaction promotes the lateral spreading of the coolant and supports the pedestal protection.

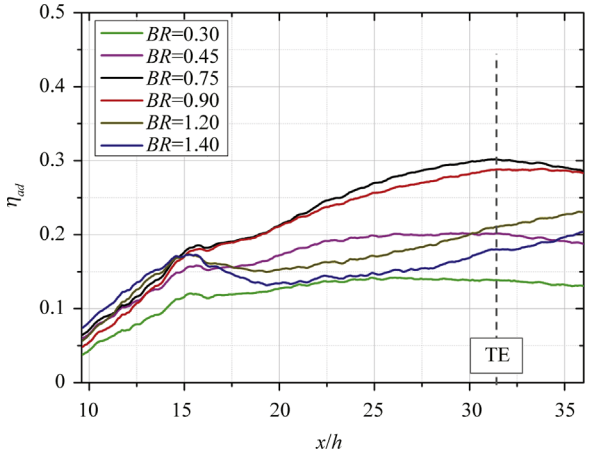

Figure 9 Geometry G0 spanwise averaged adiabatic effectiveness, only on pedestal area, for different *BR* conditions.

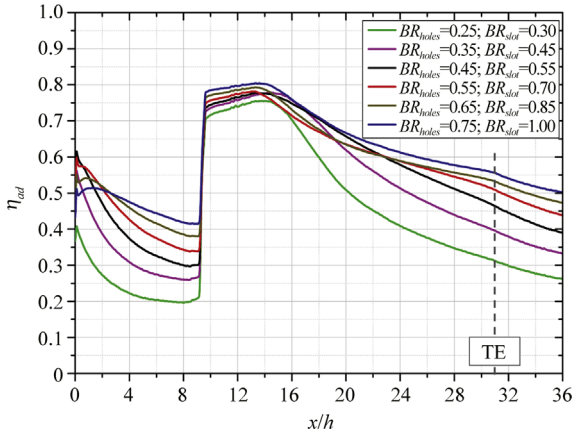

Figure 11 Geometry G1 Spanwise averaged adiabatic effectiveness, including slots and pedestals, for different *BR* conditions.

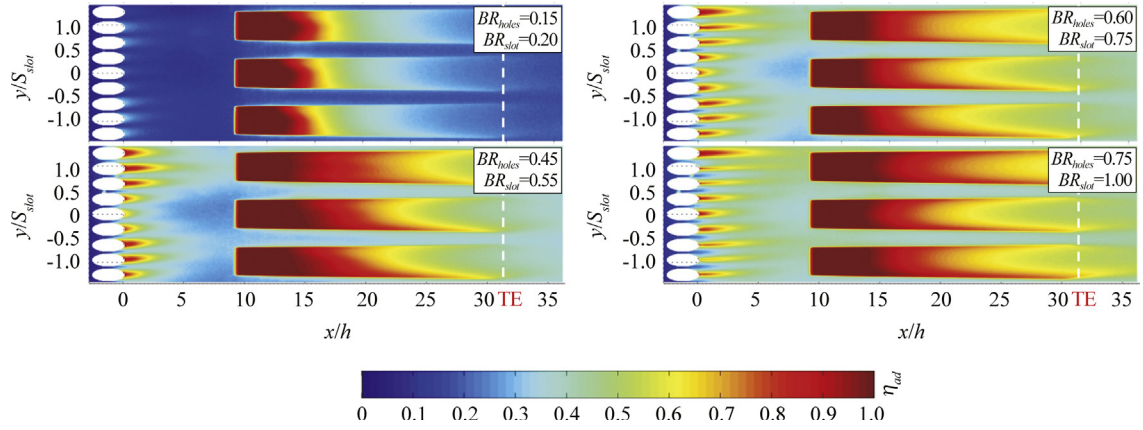

Figure 10 Adiabatic effectiveness 2D distributions (G1).

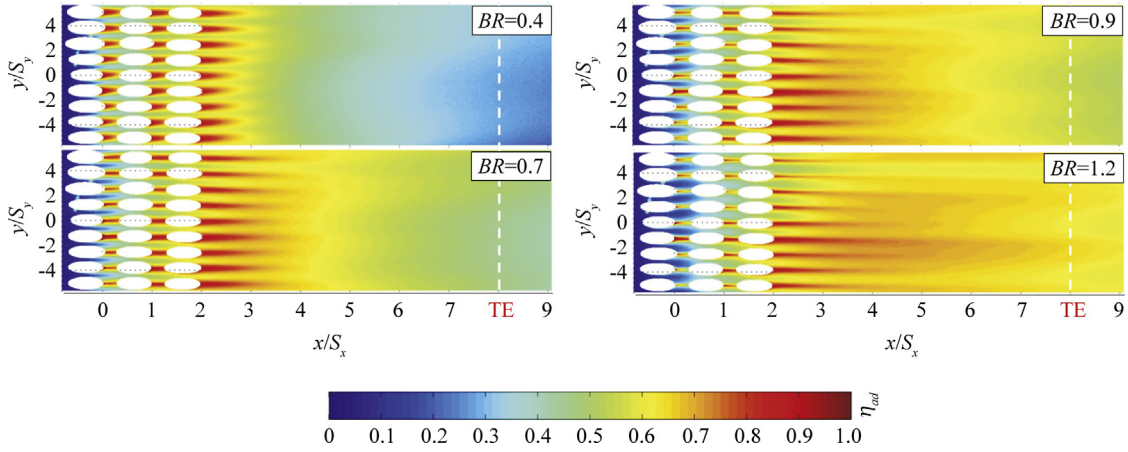

Figure 12 Adiabatic effectiveness 2D distributions (G2).

3.2. Geometry G1

The bi-dimensional distributions of adiabatic effectiveness on the central zone of geometry G1 is reported in Figure 10. Downstream the film holes, the adiabatic effectiveness distributions are characterized by a non-uniform behavior across the span direction due to the battery of pin fins in the feeding channel. As a general result for this starting zone, high *BR* values allow a better and more uniform protection. Regarding the region downstream the slot exit, it possible to identify once again a core region with high adiabatic effectiveness. With respect to geometry G0, a better protection of the pedestal outer surface is visible for all the flow conditions thanks to the coolant injected by the holes located upstream.

In the starting region downstream the film holes, the spanwise averaged adiabatic effectiveness curves (Figure 11) highlight a moderate protection of the test surface. In the range $0.15 < BR_{holes} < 0.45$ the adiabatic effectiveness trends generated by the film holes show a similar streamwise decay shape and the peak of effectiveness is located near the hole rim at $x/h = 0$. As the blowing ratio increases above the condition $BR_{holes} = 0.45$, the results show a reduction of film covering near the hole exit and the peak of effectiveness shifted towards the rig outlet; however, due to the higher coolant mass flow injected, the film effectiveness is enhanced downstream.

Regarding the film effectiveness generated by the slot, results show a non-monotonic trend varying the blowing ratio downstream the high effectiveness core region due to the strong interaction between coolant and main flow, as described for the test model G0. At the value of the x coordinate representing the trailing edge ($x/h \approx 31$) the best film protection is registered for the maximum coolant consumption condition ($BR_{holes} = 0.75$; $BR_{slot} = 1$).

3.3. Geometry G2

As reported for the previous geometries, the 2D effectiveness distributions, for several conditions of *BR*, are illustrated in Figure 12. An increase of *BR* leads to higher penetration of the jets, which in turn conducts to sharper but longer coolant traces and, in general, to a better film protection downstream the third row of holes thanks to the film superposition. At the trailing edge, the lateral

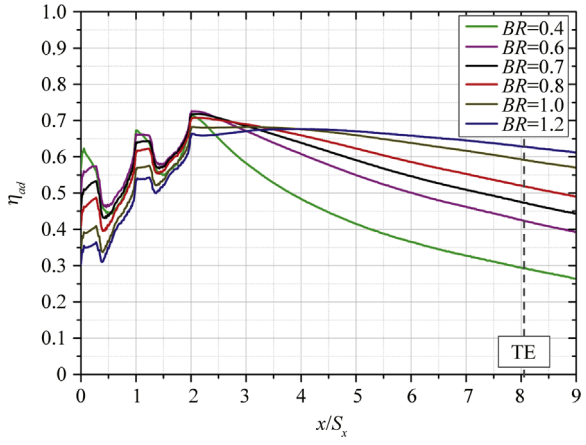

Figure 13 Geometry G2 spanwise averaged adiabatic effectiveness, including slots and pedestals, for different *BR* conditions.

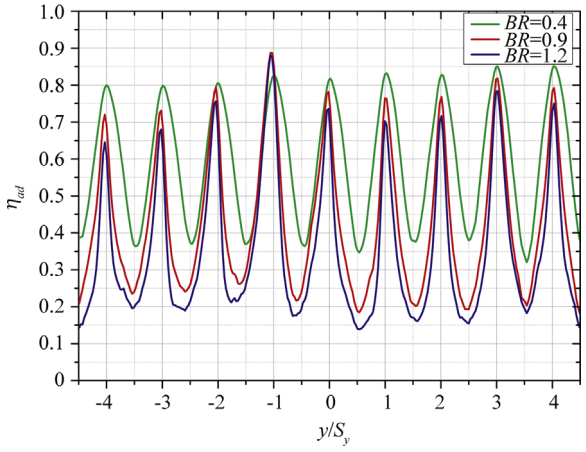

Figure 14 Geometry G2 adiabatic effectiveness spanwise profile at $x/S_x \approx 0.2$,

spreading of the coolant jets allows to obtain a more uniform effectiveness distribution in the spanwise direction and the jet traces are less intense with respect to the first part of the plate.

The spanwise averaged effectiveness curves reported in Figure 13 confirm the results suggested by the 2D maps: downstream the last row of holes, the film protection is supported by an increase of the blowing ratio condition thanks to the higher coolant mass flow injected. Opposite behavior can be observed directly downstream the first row of holes, here the limited jet penetration of the lower *BR* conditions drives to higher effectiveness values.

The adiabatic effectiveness profiles extracted at $x/S_x \approx 0.2$ (Figure 14) allow to appreciate the effect of blowing ratio parameter on the shape of the coolant traces: an increase of *BR* parameter causes a reduction of the peak level of effectiveness, located in-line with the film holes, while the coolant traces become less widespread along the spanwise direction.

3.4. Correlative analysis

To extend the validity of the survey a comparison between adiabatic effectiveness measurements and a prediction by correlative approach has been carried out on the G0 and G1 models; the final aim is to test the applicability of the superposition method proposed by Sellers [17] in case of multiple injection through holes and TE cutback with consequently strong interaction between mainstream and coolant flow. The results of this analysis is of outstanding importance when, in the first phases of the cooling system design, correlations are extensively used to predict the film effectiveness.

First of all, the experimental data for several *BR* conditions for the holes region of G1 geometry ($0 < x/h < 8$) have been compared with the results extrapolated by the correlation proposed by Baldauf et al. [26].

Figure 15 shows a good agreement, for both low and high *BR* values, between the experimental spanwise average effectiveness curves and the numerical data.

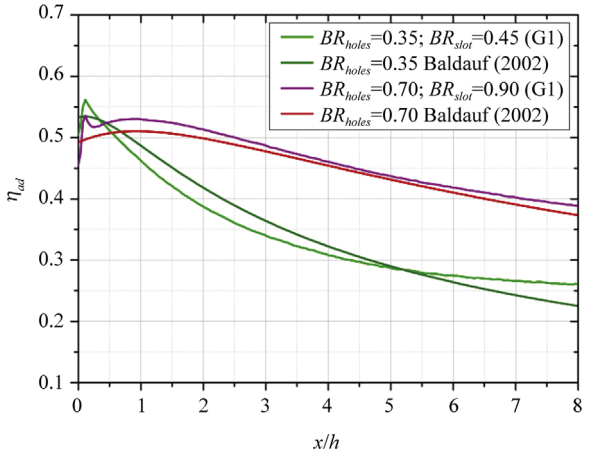

Figure 15 Geometry G1 (only holes region) spanwise averaged adiabatic effectiveness. Comparison between experimental results and numerical correlation data.

The results of this first comparison allowed to use the correlation of Baldauf et al. [26] as a robust methodology to predict the contribution to the global film effectiveness of the coolant injected from the row of holes up to the end of the test model, as prescribed by the Sellers [17] approach.

Employing Sellers superposition method, the total adiabatic effectiveness, including the multiple effect coolant injected through film holes and blade cutback, has been estimated for geometry G1. The evaluation has been carried out using the equation:

$$\eta_{ad} = \eta_1' + \eta_2' \cdot (1 - \eta_1') \tag{7}$$

where η_1' represents the film protection, extended to the entire test surface, due to the row of holes calculated by means of Baldauf correlation; while η_2' represents the effectiveness of the slot system obtained from the experimental campaign on G0 model reported in details in Figure 7. Results for $BR_{slot}=0.75$ test case (Figure 16) show the capability of Sellers superposition criterion to catch the system behavior, reproducing with good agreement the experimental trend obtained for G1. The maximum difference between

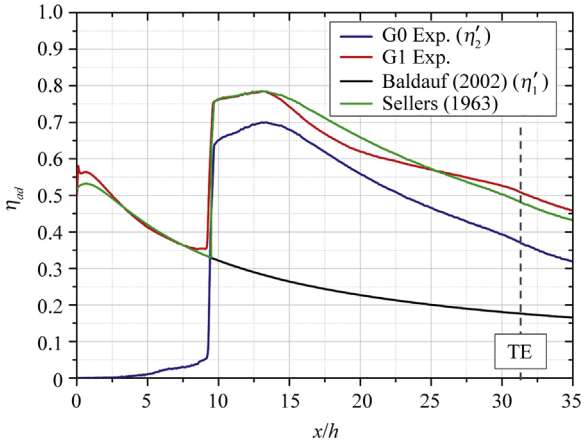

Figure 16 Spanwise average adiabatic effectiveness distributions for $BR_{slot}=0.75$. Comparison between experimental data (G0 and G1) and correlative analysis results.

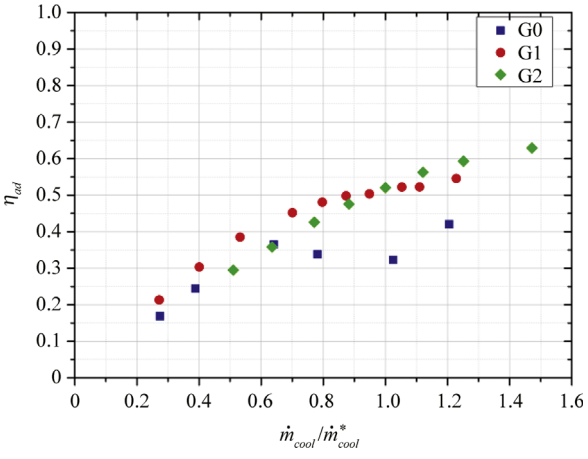

Figure 17 Spanwise average adiabatic effectiveness at TE ($x/h=31.6$) for the three geometries.

experiments and 1D methodology is in the order of 5% at $x/h \approx 18$. Similar results have been obtained also for the other test conditions investigated.

3.5. Comparison between TE models

In order to point out the actual thermal performances of all the tested configurations, normalizing the weight of coolant consumption, the spanwise averaged adiabatic effectiveness values, evaluated at the streamwise coordinate representing the blade trailing edge ($x/h = 31.6$, $x/S_x = 8$), are computed and reported in Figure 17. Results are presented as a function of the cooling mass flow normalized with a reference coolant mass flow $\dot{m}^*_{cool}$ measured for model G2 at $BR = 0.8$.

At this reference condition the model G0 works at $BR = 1.2$, while the cooling system of geometry G1 has an average blowing ratio of $BR_{slot} = 0.85$ and $BR_{holes} = 0.65$.

The configuration G0 leads to the lowest level of protection around the nominal condition and represents the only geometry that shows a non-monotonic trend of adiabatic effectiveness with varying the coolant mass flow. This behavior is ascribable to the strong unsteady interactions between cooling flow and mainstream approaching $BR = 1$, that lead to a reduction of the effective core region enhancing the decay of film effectiveness.

For $\dot{m}_{cool}/\dot{m}^*_{cool} < 1$ higher values of η_{ad} are attributable to test model G1 while the geometry G2 shows lower values due to the short coolant traces that do not reach the TE zone. However, increasing the coolant consumption over the reference condition, the trend for model G2 exhibits the best average effectiveness values thanks to the film superposition that enhances the film covering far downstream the rows of holes when the coolant jets work at high values of blowing ratio ($BR_{holes} > 1$).

The spanwise average effectiveness curves at reference condition ($\dot{m}_{cool}/\dot{m}^*_{cool} = 1$) for the three geometries are depicted in Figure 18. Geometry G0 shows lower cooling performance with respect to the other models on the entire test surface. On the other hand, the geometry G2 leads to a generally better protection in the holes region, except for a small region in the first part of the test model ($x/h < 3$). In fact at the reference coolant condition, the holes of the configuration G2 works at an high value of BR with respect to the holes of geometry G1, promoting the film covering. Directly downstream the cutback ($10 < x/h < 20$), the presence of the high effectiveness core region for the geometry G1 allows to achieve the highest effectiveness values. However, the more rapid decay of slot film covering drives to a similar trend for the models G1 and G2 approaching the exit region. At the trailing edge a slightly higher protection is achieved by the test model G2, moreover it shows a more uniform adiabatic effectiveness distribution in spanwise direction.

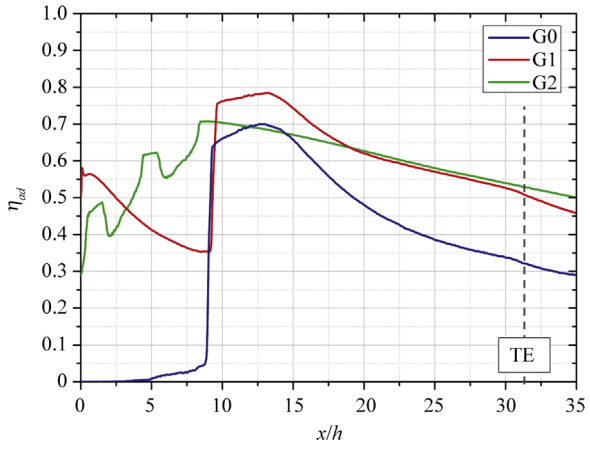

Figure 18 Adiabatic effectiveness for the three geometries at nominal coolant consumption condition ($\dot{m}_{cool}/\dot{m}^*_{cool} = 1$).

4. Conclusions

An experimental campaign has been performed in order to assess the film cooling behavior at airfoil trailing edge considering three different pressure side cooling scheme configurations. For this reason, a new test rig has been designed and commissioned to perform adiabatic effectiveness measurements using the pressure sensitive paint technique. The test rig is an open loop suction type test rig with a constant test section area which allows to replicate the Reynolds and the blowing ratio of the cooling system, and a density ratio of 1.52. The pressure sensitive paint technique was able to capture detailed 2D maps; this novel technique relying on heat and mass transfer analogy avoids inherent problems associated with conventional heat transfer methods and thus allows reducing measurement uncertainties.

First TE model tested (G0) represents the pressure side cutback of turbine airfoils and it is characterized by slots with elongated pedestals. The cooling scheme has been tested imposing several values of blowing ratio in the range 0.3-1.4. The analysis of results pointed out the effect of blowing ratio on cooling performance in the entire trailing edge region including the surfaces of the pedestals. In addition, the measurements reveal a minimum wall protection approaching BR around unity caused by the intensive mixing between coolant and mainstream promoted by the vortex shedding at the slot lip.

The second geometry (G1) shares the same features of the previous model including also a single row of holes with 20 deg inclination located upstream of the slot exits and two rows of staggered pin fins in the internal geometry. Thanks to the film holes a moderate protection was achieved in the region upstream the slots exit and on the pedestal surface. As general results higher values of adiabatic effectiveness and a more uniform distribution were obtained for high BR values.

The last trailing edge cooling system tested (G2) consists of three rows of in-line holes (20 deg of inclination angle). During the investigation the blowing ratio has been varied in the range 0.4-1.2, leading to holes Reynolds number values from 6000 to 18000. In comparison with the other

geometries, G2 presents a more uniform protection in spanwise direction and an higher film protection up to the end of the test plate.

In order to pointing out pros and cons of each geometry, a comparison between the results of three models in the condition of equal coolant consumption have been carried out. High protection levels have been highlighted respectively at the slot exit for model G1 and in the holes region for model G2, while geometries show a similar behavior in the TE exit region.

Finally, a comparison between adiabatic effectiveness measurements and a prediction by correlative approach is also reported for model G1. Results highlight the validity of the Sellers' superposition approach to correctly predict the film effectiveness even for test case with film holes and slots.

References

[1] D.S. Holloway, J.H. Leylek, F.A. Buck, Pressure-side bleed film cooling, part I: steady framework for experimental and computational results, ASME Turbo Expo GT2002-30471, 2002.

[2] D.S. Holloway, J.H. Leylek, F.A. Buck, Pressure-side bleed film cooling, part II: unsteady framework for experimental and computational results, ASME Turbo Expo GT2002-30472, 2002.

[3] G. Medic, P.A. Durbin, Unsteady effects on trailing edge cooling, Journal of Heat Transfer 127 (4) (2005) 388–392.

[4] H. Schneider, D. von Terzi, H.J. Bauer, Large-eddy simulations of trailing-edge cutback film cooling at low blowing ratio, International Journal of Heat and Fluid Flow 31 (2010) 767–775.

[5] J. Joo, P. Durbin, Simulation of turbine blade trailing edge cooling, Journal of Fluids Engineering 131 (2) (2009) 021102. 1-14.

[6] M.E. Taslim, S.D. Spring, B.P. Mehlman, An experimental investigation of film cooling effectiveness for slots of various exit geometries, AIAA Journal of Thermophysics and Heat Transfer 6 (2) (1992) 302-307.

[7] P. Martini, A. Schulz, H.J. Bauer, Film cooling effectiveness and heat transfer on the trailing edge cut-back of gas turbine airfoils with various internal cooling designs, Journal of Turbomachinery 128 (2006) 196–205.

[8] T. Horbach, A. Schulz, H.J. Bauer, Trailing edge film cooling of gas turbine airfoils - effects of ejection lip geometry on film cooling effectiveness and heat transfer, in: International Symposium on Heat Transfer in Gas Turbine Systems, Paper No.42-TE, Antalya, Turkey, 2009.

[9] T. Horbach, A. Schulz, H.J. Bauer, Trailing edge film cooling of gas turbine airfoils - external cooling performance of various internal pin fin configurations, Journal of Turbomachinery 133 (2011) 041006. 1-9.

[10] A. Dannhauer, Investigation of trailing edge cooling concepts in a high pressure turbine cascade: analysis of the adiabatic film cooling effectiveness, ASME Turbo Expo GT2009-59343, 2009.

[11] Z. Yang, H. Hu, An experimental investigation on the trailing edge cooling of turbine blades, Propulsion and Power Research 1 (1) (2012) 36–47.

[12] F.E. Ames, N.J. Fiala, J.D., Johnson, Gill slot trailing edge heat transfer: effects of blowing ratio, Reynolds number, and external turbulence on heat transfer and film cooling effectiveness, ASME Turbo Expo GT2007-27397, 2007.

[13] J.D. Johnson, N.J. Fiala, F.E. Ames, Gill slot trailing edge aerodynamics: effects of blowing rate, Reynolds number, and external turbulence on aerodynamic losses and pressure distribution, Journal of Turbomachinery 131 (1) (2009) 011016.

[14] N.J. Fiala, I. Jaswal, F.E. Ames, Letterbox trailing edge heat transfer: effects of blowing rate, Reynolds number, and external turbulence on heat transfer and film cooling effectiveness, Journal of Turbomachinery 132 (1) (2010) 011017.

[15] N.J. Fiala, J.D. Johnson, F.E. Ames, Aerodynamics of a letterbox trailing edge: effects of blowing rate, Reynolds number, and external turbulence on aerodynamic losses and pressure distribution, Journal of Turbomachinery 132 (4) (2010) 041011.

[16] G. Barigozzi, A. Perdichizzi, S. Ravelli, Pressure side and cutback trailing edge film cooling in a linear nozzle vane cascade at different Mach numbers, Journal of Turbomachinery 134 (5) (2012) 051037.

[17] J.P. Sellers, Gaseous film cooling with multiple ejection stations, AIAA Journal 1 (9) (1963) 2154–2156.

[18] A.C. Nix, A.C. Smith, T.E. Diller, W.F. Ng, K.A. Thole, High intensity, large length-scale freestresm turbulence generation in a transonic turbine cascade, ASME Turbo Expo GT2002-30523, 2002.

[19] P.E. Roach, The generation of nearly isotropic turbulence by means of grids, International Journal of Heat and Fluid Flow 8 (2) (1987) 82–92.

[20] J.R. Lakowicz, Principles of Fluorescence Spectroscopy, Springer, 2006.

[21] T.V. Jones, Theory for the use of foreign gas in simulating film cooling, International Journal of Heat and Fluid Flow 20 (1999) 349–354.

[22] G. Caciolli, B. Facchini, A. Picchi, L. Tarchi, Comparison between PSP and TLC steady state techniques for adiabatic effectiveness measurement on a multiperforated plate, Experimental Thermal and Fluid Science 48 (2013) 122–133.

[23] S.J. Kline, F.A. McClintock, Describing uncertainties in single sample experiments, Mechanical Engineering 75 (1953) 3–8.

[24] A. Bonini, A. Andreini, C. Carcasci, B. Facchini, A. Ciani, L. Innocenti In: Conjugate heat transfer calculations on GT rotor blade for industrial applications, part I: equivalent internal fluid network setup and procedure description, ASME Turbo Expo GT2012-69846, 2012.

[25] L. Andrei, A. Andreini, B. Facchini, L. Winchler, A decoupled CHT procedure: application and validation on a gas turbine vane with different cooling configurations, Energy Procedia 45 (2014) 1087–1096.

[26] S. Baldauf, A. Schulz, S. Wittig, M. Scheurlen, Correlation of film-cooling effectiveness from thermographic measurements at enginelike conditions, Journal of Turbomachinery 124 (4) (2002) 686–698.